ADVANCED FUNCTIONAL MATERIALS
www.afm-journal.de

Simultaneous Culturing of Cell Monolayers and Spheroids on a Single Microfluidic Device for Bridging the Gap between 2D and 3D Cell Assays in Drug Research

*Päivi Järvinen, Ashkan Bonabi, Ville Jokinen, and Tiina Sikanen**

Two-dimensional (2D) cell cultures have been the primary screening tools to predict drug impacts in vitro for decades. However, owing to the lack of tissue-specific architecture of 2D cultures, secondary screening using three-dimensional (3D) cell culture models is often necessary. A microfluidic approach that facilitates side-by-side 2D and 3D cell culturing in a single microchannel and thus combines the benefits of both set-ups in drug screening; that is, the uniform spatiotemporal distributions of oxygen, nutrients, and metabolic wastes in 2D, and the tissue-like architecture, cell–cell, and cell–extracellular matrix interactions only achieved in 3D. The microfluidic platform is made from an organically modified ceramic material, which is inherently biocompatible and supports cell adhesion (2D culture) and metal adhesion (for integration of impedance electrodes to monitor cell proliferation). To induce 3D spheroid formation on another area, a single-step lithography process is used to fabricate concave microwells, which are made cell-repellant by nanofunctionalization (i.e., plasma porosification and hydrophobic coating). Thanks to the concave shape of the microwells, the spheroids produced on-chip can also be released, with the help of microfluidic flow, for further off-chip characterization after culturing. In this study, the methodology is evaluated for drug cytotoxicity assessment on human hepatocytes.

1. Introduction

3D in vitro cell culturing techniques have received increased recognition in drug screening and validation during the last decade. In 3D, the cells retain organ-specific functions better than in 2D cell cultures,[1–4] which often improves the in vitro–in vivo correlation of the drug safety and efficacy assessment.[1,5] For example, significantly increased drug resistance (over 2D cell cultures) has been reported to cisplatin and paclitaxel in 3D spheroid cultures of ovarian cancer cell lines[2] as well as to doxorubicin in 3D spheroid cultures of breast cancer cell lines.[6] For instance, the cytotoxicity associated with drug metabolites is often underestimated in 2D cultures, because the cells grown as monolayers seldom express metabolizing enzymes at physiological levels and the polarization of the drug transporter proteins is often impaired.[7] 3D cell cultures can be established by a variety of techniques, including forced floating in hanging drops or U-shaped, low-attachment microwell plates that promote formation of compact spheroids,[8] as well as by employing hydrogels or other matrices that support 3D architecture for embedded cells.[9] The lack of standardization, however, results in some challenges. For example, the increasing focal length and consequent light scattering are problematic for the detection of large spheroids (∅ > 150 µm) and thick matrix specimens, and may necessitate the use of clearing agents to improve deep specimen resolution,[10] which inevitably increases the workload associated with 3D cultures.

Microfluidics is increasingly exploited to cell culturing in both 2D and 3D to better mimic the in vivo conditions in drug safety and efficacy assessment.[11–14] By providing precise spatiotemporal control over the culture conditions, microfluidics enables improved supply of nutrients and oxygen, and efficient removal of metabolic waste. These factors have immediate impacts on both the cell health and the accuracy of the in vitro-in vivo prediction of drug effects. Additionally, microfabricated cell traps (e.g., microwells) often enable production of much smaller 3D cell cultures than achievable for conventional wellplate-based culture platforms. This is particularly important to avoid the problems arising from diffusion-limited mass transfer, which may impair the penetration of antibodies, fluorophores, and other detection reagents, and thus potentially give rise to false negative or positive results, in conventional 3D cultures.[10,15,16] Most of the commonly used microfabrication methods and materials yield vertical walls, that is, cylindrical microwells,

Dr. P. Järvinen, Dr. A. Bonabi, Dr. T. Sikanen
Drug Research Program
Division of Pharmaceutical Chemistry and Technology
Faculty of Pharmacy
University of Helsinki
Viikinkaari 5E, Helsinki 00790, Finland
E-mail: tiina.sikanen@helsinki.fi
Dr. V. Jokinen
Department of Chemistry and Materials Science
School of Chemical Engineering
Aalto University
Tietotie 3, Espoo 02150, Finland
The ORCID identification number(s) for the author(s) of this article can be found under https://doi.org/10.1002/adfm.202000479.

DOI: 10.1002/adfm.202000479

which sets certain constraints to on-chip spheroid formation and culturing. In cylindrical microwells, however, the cells are initially located far apart from each other and lack cell-cell interactions during aggregation, which easily results in low reproducibility and high size variation in spheroid formation from well to well. Increasing the initial cell count or decreasing the well dimensions improves reproducibility, but simultaneously the culturing time becomes limited due to the cells outgrowing the wells. Therefore U-shaped wells are typically preferred for spheroid culturing. In U-shaped wells, the gravitational force is single-pointed, which forces the cells closer to each other even if the well size is large (as in conventional U-shaped microtiter plates). Although microfluidic flow is relatively easy to integrate with the 2D cell cultures,[13] implementation of U-shaped microwells is however significantly challenging and may require complex multistep microfabrication protocols.[17] Concave microwells can generally be fabricated either directly via, for example, isotropic etching,[18] laser ablation,[19] or milling[11] or indirectly by replica-molding from an inverse microdroplet-shaped features obtained via, for example, photoresist reflow.[20] However, most of these processes yield relatively shallow microwells, which cannot retain the growing spheroids over extended culturing periods. Moreover, most biocompatible polymers lack isotropic etching processes and the post-processing possibilities (e.g., metallization or spatioselective surface modification) of replica-molded microstructures are often limited compared with photolithographically produced microdevices.

In this paper, we describe a microfabrication method, which facilitates straightforward implementation of U-shaped microwells for production of small 3D cell spheroids under microfluidic flow. The developed microfluidic platform is made from an organically modified ceramic material (Ormocomp), which is optically transparent down to near-UV range[21] and inherently biocompatible supporting cell adhesion without any additional coating.[22–26] Thus, the developed platform also enables parallel culturing of 2D cell monolayers, under identical growth conditions to those of 3D spheroids, in a single microfluidic channel. For the fabrication of the round (cross-section profile) microwells, we exploit the controlled overexposure of Ormocomp,[27] which facilitates straightforward customization of the microwell shape and depth in a single lithographic step. To further induce 3D spheroid formation, lithographic (masked) nanofunctionalization by plasma processing is exploited to defining local cell-repellant surfaces (in the microwell arrays) via porosification and hydrophobic coating of the native Ormocomp. Thereby, the developed concept facilitates side-by-side, but isolated culturing of cells in 2D (monolayers) and 3D (spheroids) on native and modified surfaces, respectively, so as to take the best of both worlds. Namely, there are certain factors, which favor the use of 2D cell culture methodologies in parallel to 3D cultures, such as the availability of mature and standardized protocols facilitating straightforward detection of localization of target proteins within the cells as well as monitoring of cell population level events, for example, by impedance spectroscopy or fluorescence staining.[5] The concept was herein applied to drug cytotoxicity evaluation with the help of paclitaxel, a known hepatotoxic anticancer drug.

2. Results and Discussion

2.1. The Concept of Parallel Culturing of Cell Monolayers (2D) and Cell Spheroids (3D) on Chip

The microfluidic platform designed herein comprises of three arrays of concave microwells that have cell-repellent, hydrophobic surface properties (3D cell culture vessels) and planar zones of native Ormocomp that supports cell adhesion (2D cell monolayer culturing) (**Figure 1** and Figure S1, Supporting Information). In addition, the platform comprises of two sets of thin-film gold electrodes patterned onto the planar, native Ormocomp areas and facilitates monitoring of the cell growth and integrity in monolayer cultures by impedance spectroscopy. The microfluidic control of growth conditions is achieved by sealing the Ormocomp platform with a gas-permeable polydimethylsiloxane (PDMS) channel (200 μm × 3 mm × 30 mm, height × width × length) (Figure 1a–c). With this setup, the cell loading, seeding, flushing of the excess cells, and cell culturing are all performed on-chip sequentially, and most importantly, can be done simultaneously for both 2D and 3D cultures (Figure 1c). This guarantees that the conditions are exactly the same for both culture types.

In this study, the well geometry (depth and shape) was optimized to enable trapping of a large enough population of cells to induce cell aggregation, but small enough to leave sufficient room for spheroid growth over time (Figure 1d). When using the stopped flow approach for cell seeding, the number of trapped cells in each microwell was linearly proportional to the well size ($y = 0.34x$-26.58, $R^2 = 0.9908$, Figure 1e). To prevent cell adhesion, both inside the wells and around the well array (Figure 1f), the Ormocomp surface was made locally hydrophobic and nanoporous by plasma treatments, which have been shown to reduce cell adhesion in previous literature.[28,29] On the untreated, planar areas, the native Ormocomp surface supported strong adhesion of both cells (Figure 1f) and metals (Figure 1g), which facilitated integration of cell-compatible gold electrodes for impedance detection. The cell compatibility of native Ormocomp[22–26] as well as the Ormocomp metallization protocols[30] has been thoroughly established in previous literature. In this study, the impedance spectra were measured after cell seeding, once every hour for 96 h, using frequency range of 5–100 000 Hz (Figure 1h). The increase in impedance signal at the optimized frequency of 16 kHz was in good agreement with the optically observed increase in cell confluence on top of the gold electrodes (see Figure S2, Supporting Information). On the cell monolayer (2D) culture, 80% confluence was achieved within ca. 48 h (see Figure S2, Supporting Information). Critical to the assay performance was also to ensure effective isolation of the monolayer and spheroid cultures from each other. In the next section, the validation of the microfabrication protocol is described in more detail to illustrate how the initial spheroid size can be effectively controlled by microfabrication means and how the employed lithographic processes enable fabrication of sharp borders between the cell-adhesive and cell-repellant areas, so that no cells adhere onto the porosified, hydrophobic area separating the 2D and 3D cultures (Figure 1f).

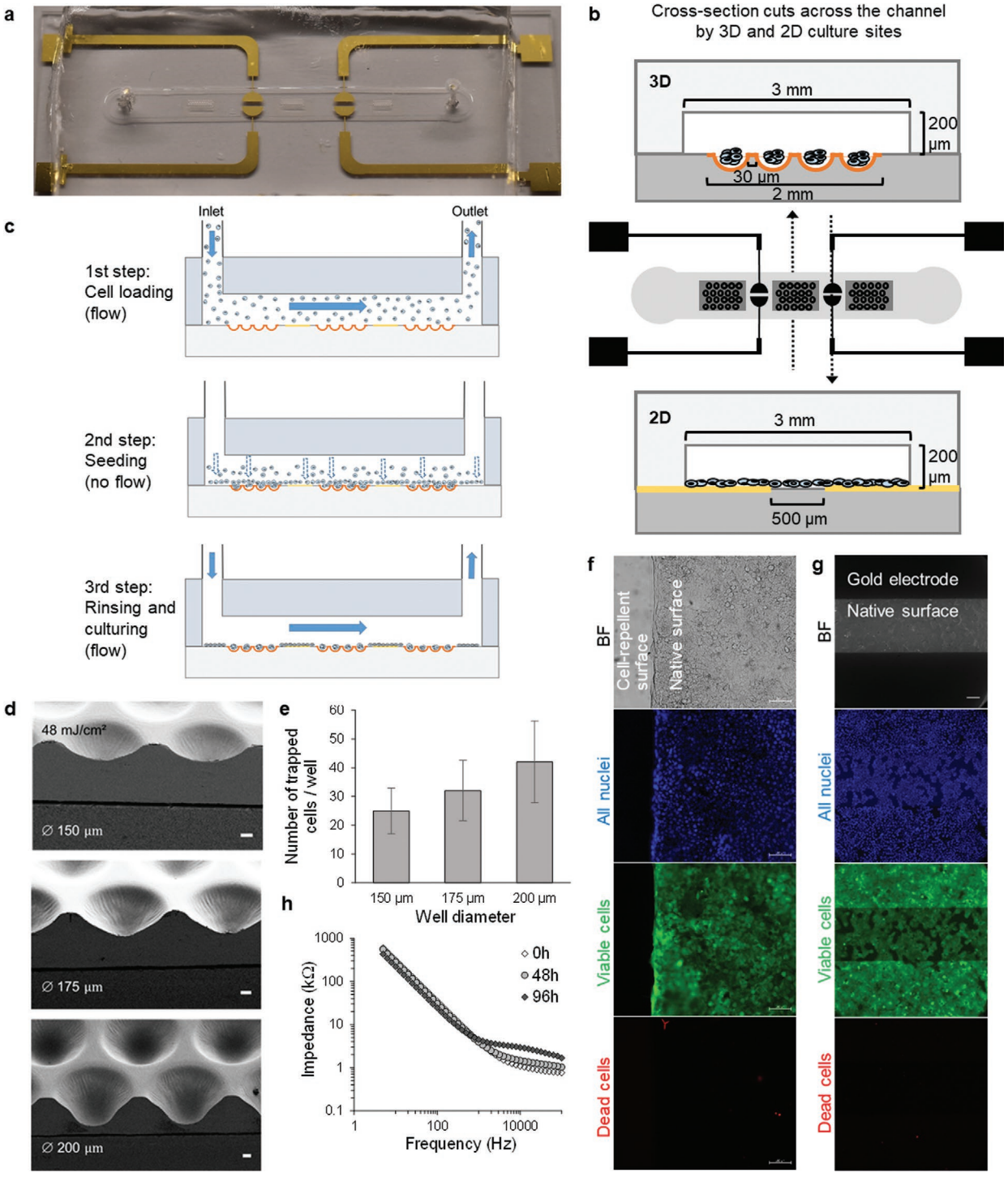

Figure 1. The assay set-up for the microfluidic side-by-side 2D and 3D cell culturing device. a) Picture of the chip. b) A diagram of the functional units and cross-section cuts across the microchannel at the points of 3D and 2D culturing (cross-cut locations indicated in diagram). c) A cross-section cut of the Ormocomp-PDMS-chip along the microchannel with illustrations of the sequential cell seeding steps: 1) cell loading, 2) seeding of cells during 30 min under static conditions, and 3) flushing of the excess cells and culturing of the cell monolayers and spheroids under microfluidic flow (5.8 mm min^{-1} for the first 8 h, thereafter 2.3 mm min^{-1}). d) The impact of the nominal microwell diameter (on the photomask) on the resulting microwell cross-section profile at constant UV dose of 48 mJ cm^{-2}. Scale bars 20 µm. e) The impact of microwell diameter (nominal) on the number of trapped cells (mean ± SD, $n > 12$ microwells of each size, three independent experiments, 2.5 M cells mL^{-1}). f) The impact of surface modification on the cell adhesion illustrating sharp edge of the cell monolayer culture at 96 h. Cell-repellent: hydrophobic and porous. Native: hydrophilic and nonporous. g) Cells cultured (48 h) on top of the gold electrodes indicating uniform monolayer formation. h) The on-chip impedance spectra of the 2D cell culture recorded at 0-48-96 h indicating increased impedance at around 16 kHz as the result of cell proliferation and maturation of the cell–cell junctions. The cell stains in (f,g): Hoechst 33342 (blue), Calcein AM (green) and PI (red). Scale bars 100 µm. Illustrations in (b–c) are not in scale.

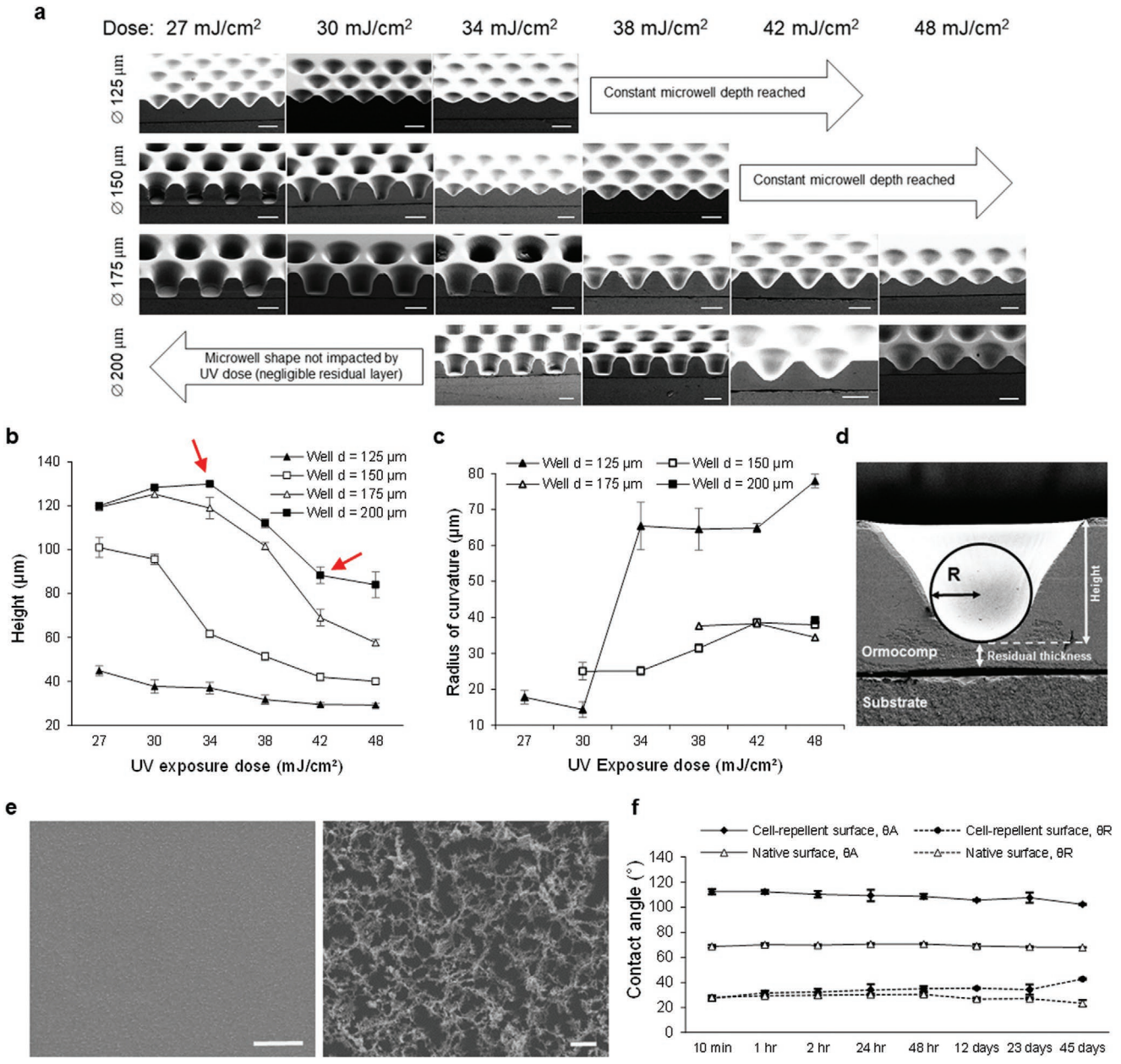

Figure 2. The impact of UV exposure dose on a) the evolution of the microwell shape illustrated in SEM images (scale bars 100 µm), b) the microwell height measured by profilometer (mean ± SD, $n = 3$), arrows pointing the linear area in 200 µm wells, and c) the radius of the curvature determined from SEM images (mean ± SD, $n = 4$) as illustrated in figure (d). e) The impact of plasma porosification on the Ormocomp surface: nonporous (left) and porous (right). Scale bars 2 µm. f) The stability of the advancing (θ_A) and receding (θ_R) contact angles of native, cell-adhesive (hydrophilic, non-porous), and treated, cell-repellent (porosified, fluoropolymer coated) Ormocomp surfaces as a function of time ($n = 3$ measurements each).

2.2. Validation of the Microfabrication Method

The detailed microfabrication process is described in the Experimental section and illustrated in Figure S1, Supporting Information. Briefly, the depth and cross-section shape of the microwells is defined by the UV exposure dose (in a single lithographic step), which has been previously applied to fabrication of round (cross-section) microchannels for optical applications.[27] The evolution of the microwell cross-section shape from rectangular to rounded shape upon increasing UV dose is illustrated in **Figure 2**a. After reaching a well-diameter-dependent threshold dose, the thickness of the residual layer at the bottom of the microwell increases linearly as a function of UV dose resulting in linearly decreasing microwell depth until a saturation level, that is, constant microwell depth, is reached (Figure 2b). In addition to depth, the impact of the UV dose on the microwell cross-sectional shape was quantified with the help of a circle fit to scanning electron micrographs (SEM) in Matlab (Figure 2c,d). Generally, lower exposure doses resulted in a U-shaped cross-section profile and higher doses in a

semicircular profile. The required dose was however dependent on the microwell diameter (Figure 2a). In this study, an exposure dose of 48 mJ cm^{-2} was used in all subsequent experiments since it provided rounded cross-sectional profile for the largest microwell sizes ranging from 150 to 200 µm in diameter (Figures 1d and 2a). Under these conditions, the microwell volume and the aspect ratio (w × h) could be optimized with a view to trapping of desired initial amount of cells during seeding and to hold the growing spheroids in the microwells over extended periods of time. Most importantly, the lithography-based manufacturing of microwells is readily compatible with the subsequent lithographic (masked) surface functionalization, which herein was a combination of oxygen plasma porosification similar to Aura et al.[31] (Figure 2e) and plasma-enhanced chemical vapor deposition of fluoropolymer. Since both surface modifications were applied in a single lithography step, they were perfectly aligned with each other facilitating a clear change in the surface wettability compared with the native Ormocomp surface. As the result of the treatments, the advancing water contact angle increased from 69 ± 1° (native) to 112 ± 2° (modified), and the altered surface properties were shown to be stable over at least one month (Figure 2f). However, the surface treatments did not significantly affect the receding contact angle (native 28 ± 1° versus modified 27 ± 1°), indicating that some hydrophilic moieties were left on the modified surfaces as well. Altogether, these properties resulted in effective cell repellence on the modified surfaces.

2.3. Characterization of the 3D Spheroid Formation on Chip

The feasibility of the developed Ormocomp chip for culturing of 3D cell spheroids was examined with human hepatocytes seeded into the hybrid Ormocomp-PDMS channel (Huh7, 2.5 M mL^{-1} in complete growth medium). In these experiments, three arrays of 4 × 10 microwells, each featuring different, but constant (within array) microwell diameters, that is, 150, 175, and 200 µm, were incorporated into a single microchannel. The hydrophobic and nanoporous surface (in the microwell area) was able to resist cell adhesion for at least 30 min, which was the duration of the static cell seeding step in this study and sufficient to ensure strong enough cell adhesion onto native Ormocomp areas and cell sedimentation into the microwells. After cell seeding, a flow of complete medium, supplemented with 2% (*v*/*v*) Geltrex to provide with soluble extra cellular matrix (ECM) components, was applied at a flow rate of 5.8 mm min^{-1} (0.033 dyne cm^{-2}) for the first 8 h to ensure removal of unadhered cells from the channel. Thereafter, the cell culture was maintained under constant flow of 2.3 mm min^{-1} (0.012 dyne cm^{-2}). The spheroid growth over time (3D culture) is illustrated in **Figure 3**a,b. In the 150 µm (nominal i.d.) microwells, the lift force induced by the microfluidic flow resulted in premature release of the outgrowing spheroids, but in the 175 and 200 µm (i.d.) microwells, the spheroid size was shown to increase linearly over time for at least 96 h (Figure 3b). Besides culturing time, the spheroid size was dependent on the microwell diameter, that is, the initial number of trapped cells (Figure 1e). As expected, the initial cell number required to produce compact spheroids within 24 h was substantially lower compared with previous work employing cylindrical microwells (flat bottom, vertical sidewalls, e.g., Patra et al.[12]).

In addition to spheroid formation, the round (cross-section) microwell shape was critical to facilitating controlled release of the on-chip cultured spheroids for further off-chip characterization, which is not as easily achieved when using cylindrical microwells. The fact that most microfluidic 3D cell cultures only enable on-chip (in situ) cell analysis, and thus, omit the possibility to use the state-of-the-art "off-chip" cell characterion techniques (e.g., flow cytometry, light sheet microscopy, or optical projection tomography) is currently one of the major hurdles of microfluidic 3D cell culturing. Detailed characterization of the 3D shape and size of the formed spheroids is particularly important when introducing new cell lines, because of reported differences in spheroid formation between different cell types.[8] In this study, the shape and size of the on-chip cultured hepatocyte spheroids were determined in more detail by light sheet microscopy (off-chip analysis) to supplement the in situ characterization by optical microscopy. For this purpose, new microfluidic designs incorporating only one size of microwells per each channel were fabricated to enable culturing of batches of uniform spheroids. This design incorporated total of 340 microwells (ca. 19 wells mm^{-2}). After day 4, the spheroid size typically exceeded the threshold value for retention (e.g., ca. 160 µm spheroid size in ∅200 µm microwells), which facilitated easy release of the spheroids from the concave microwells with the help of the lift force induced by the fluid flow. The light sheet microscopy confirmed that the spheroids formed in the Ormocomp microwells were symmetrical (sphericity of 0.97 ± 0.01, Figure 3d) and exhibited organized cellular hierarchy with cortically localized filamentous actin (Figure 3e). These results thereby evidenced that the spheroid architechture was truly 3D and qualified the use of the spheroid diameter (determined in situ based on optical microscopy) as a representative measure of the spheroid growth in further method validation studies.

2.4. Method Validation for Drug Cytotoxicity Screening

The impact of drug exposure on the parallel 2D and 3D hepatocyte cultures was examined with the help of a known hepatotoxic anticancer drug, paclitaxel. Paclitaxel is known to cause cell cycle arrest into the G2/M phase by binding to β-tubulin, which leads to kinetic stabilization of mitotic spindle microtubule dynamics, and further, to deformation of nuclei and growth arrest.[32] Also in the control experiments (2D cell cultures on microtiter plates) performed in this study, paclitaxel was shown to cause a time- and dose-dependent cell cycle arrest (**Figure 4**a and Figure S3, Supporting Information). On the microfluidic platform, the impact of paclitaxel exposure on the 3D spheroid growth was assessed based on spheroid diameter (in situ determination by optical microscopy), and on the cell monolayer (2D) integrity based on on-chip impedance spectroscopy. As a result of paclitaxel exposure (100 and 1000 nM), a clear dose-dependent inhibition of the 2D and 3D cell growth was detected in the on-chip impedance signal (Figure 4b) and in the spheroid size (Figure 4c, Tables S1,S2, Supporting Information), respectively. In both cases, the high

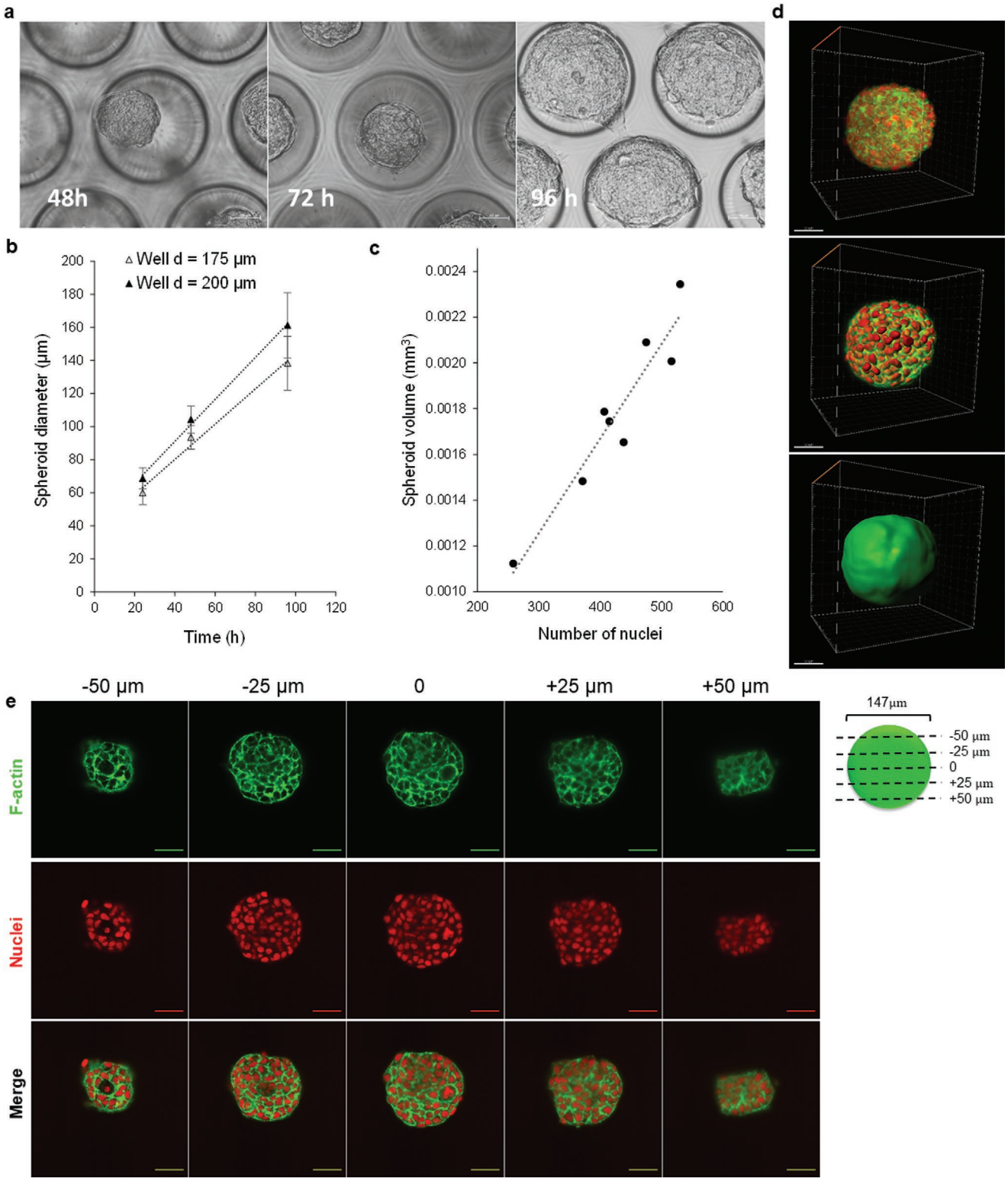

Figure 3. Characterization of Huh7 spheroids grown in concave microwells in Ormocomp channel under flow conditions. a) Spheroid growth in 200 µm wells over time (48-72-96 h). b) Linear growth of spheroids in both 175 and 200 µm wells over time ($R^2 = 0.9885$ and 0.967 for 175 and 200 µm well, respectively, mean ± SD, $n > 12$, three independent experiments). c) Correlation of spheroid volumes and number of nuclei (Pearson's correlation 0.951, $p < 0.01$) analyzed using light sheet microscope Z-stack images and IMARIS analysis software. d) 3D construct of merged channels (actin, green; and nuclei, red) (top), analysis of nuclei surfaces (middle), and surface of the whole spheroid volume (bottom). e) Inner spheroid structural details of the actin and nuclei alignment from selected Z-heights indicated in diagram. (c,d) The 3D constructs created from 0.47 µm thick Z-stack images. a,d,e) Scale bars 50 µm.

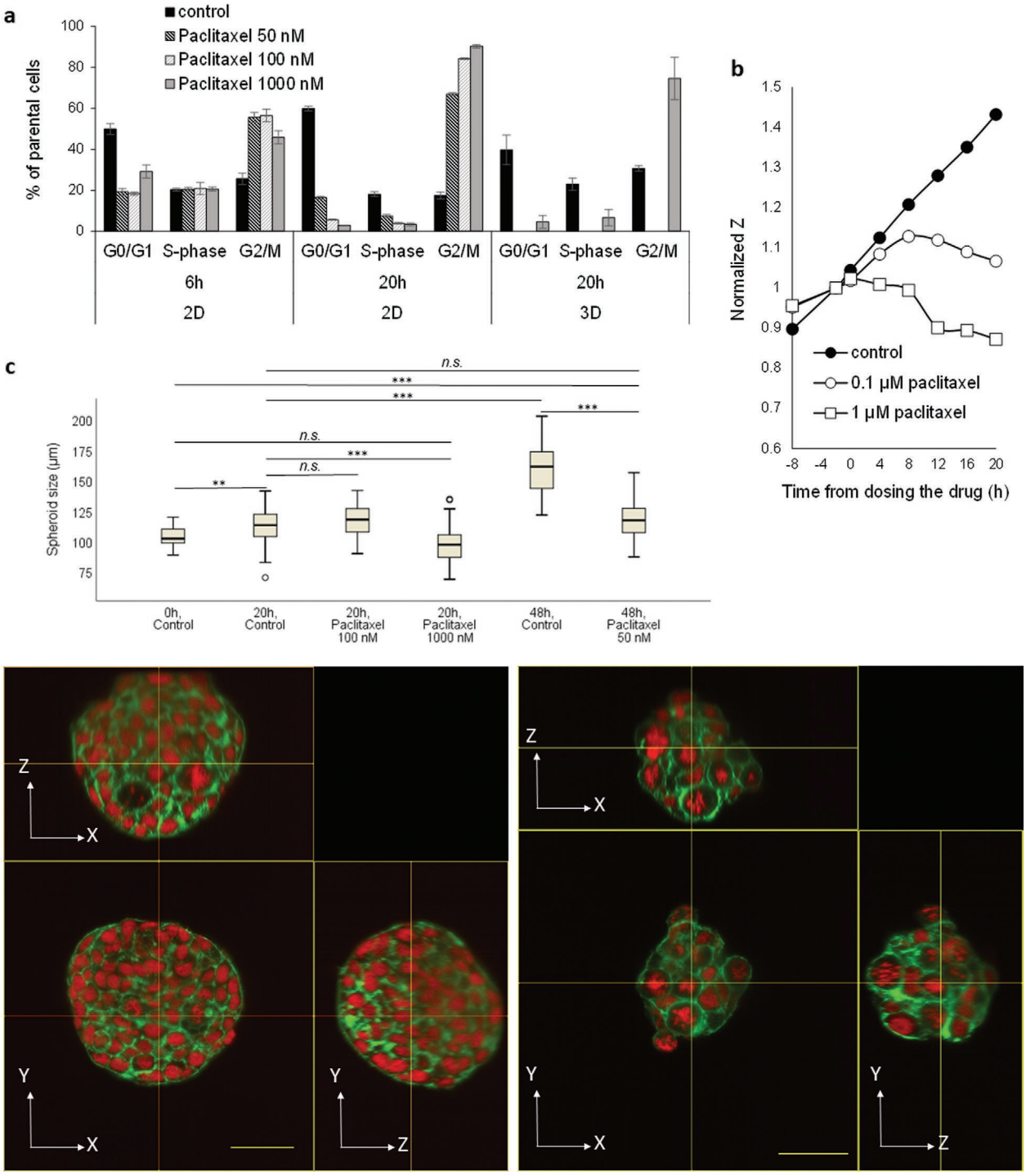

Figure 4. Validation of parallel cell culturing set-ups. a) Paclitaxel induced, time-dependent cell cycle arrest in G2/M-phase in Huh7 cells in a 2D cell culture on the standard 96-well plate, and in 3D spheroids cultured on-chip. The data represents the mean ± SD from $n = 3$ repeated experiments. b) Disruption of the cell monolayer integrity (2D) observed on the on-chip impedance sensor at 16 kHz. The impedance signal was normalized to the signal obtained two hours ($t = -2$ h) before dosing the drug ($t = 0$ h). Baseline impedance values at time 0 h (the time of dosing the drug) were 2108 Ω for control (medium) and 1366 and 1458 Ω for cell monolayers exposed to 100 and 1000 nM paclitaxel, respectively. c) The effect of paclitaxel on spheroid size. Paclitaxel was introduced at 48 h (0 h post-exposure) and drug effects were evaluated at 20 or 48 h post-exposure (mean ± SD). Number of characteristic measures (two characteristic measures of diameter/spheroid): $n_{0\text{ h, control}} = 62$, $n_{20\text{ h, control}} = 60$, $n_{20\text{ h, paclitaxel 100 nM}} = 68$, $n_{20\text{ h, paclitaxel 1000 nM}} = 68$, $n_{48\text{ h, control}} = 73$, $n_{48\text{ h, paclitaxel 50 nM}} = 307$. Pair-wise comparison of independent samples based on Kruskal–Wallis test. $p < 0.05$ was considered to be statistically significant difference, and also the limits of $^{**}p < 0.01$ and $^{***}p < 0.001$ were evaluated. *n.s.* = non-significant. d) Orthogonal projections of a control spheroid, not exposed to paclitaxel (left) and spheroid exposed to high dose (500 nM) of paclitaxel for 48 h (right) corresponding total culturing time of 96 h. Spheroids were fluorescent-labeled for F-actin (Actin-Green, green) and nuclei (DRAQ-5, red). Scale bars 50 µm.

paclitaxel dose (1000 nM) terminated the cell proliferation instantly. The post-exposure size of the spheroids in the presence of 1000 nM paclitaxel at 20 h (i.e., after one post-exposure cell cycle) was 99 ± 14 µm (n = 34), which was similar to that before the exposure (104 ± 8 µm, n = 31) indicating immediate termination of the cell proliferation (Figure 4c). The cell cycle arrest was further confirmed by off-chip cytometric analysis of the propidium iodide (PI) stained cells (dissociated spheroids). When exposed to 1000 nM paclitaxel the proportion of spheroid cells in G2/M phase (74.6 ± 10.3%) was comparable to the value (90.2 ± 0.8%) obtained from the conventional 2D culture (Figure 4a). Instead, when exposed to a lower dose of paclitaxel, the spheroids continued to grow, and the impact of paclitaxel could not be seen yet after 20 h exposure period. After the first 20 h of paclitaxel exposure (100 nM), the spheroid size (118 ± 12 µm, n = 34) did not significantly differ from that of the control (114 ± 14 µm, n = 30) (Figure 4c). In the 2D culture, however, the lower paclitaxel dose (100 nM) retarded the cell growth in a time-dependent manner with lag time of ca. 8 h compared with the high dose (1000 nM) suggesting that some of the cells continue to proliferate even upon paclitaxel exposure if the dose is sufficiently low (time-dependent cell-cycle arrest). This observation is well in line with the previous literature, which describes a time-dependent inhibition of cell proliferation at notably low concentrations as a result of paclitaxel accumulation in cells. For example, the IC50 value of paclitaxel in HeLa cells is ca. 8 nM only.[32] To further evaluate the feasibility of the developed platform for detection of such time-dependent drug impacts, the 3D spheroid culture was exposed to 50 nM paclitaxel concentration, which was well below the threshold of acute cytotoxicity on the basis of the afore-mentioned short-exposure experiments with microfluidic 3D and 2D cultures. To ensure sufficiently good signal window (here, the Z' factor was 0.8), exposure time of 48 h was used to assess the impact of paclitaxel at lower doses. Under these conditions, the post-exposure (50 nM paclitaxel, 48 h) spheroid size was 118 ± 14 µm (n = 153), which corresponds to ca. 27% of the growth of the control spheroids (161 ± 20 µm, n = 36) grown for the same period of time (total of 96 h) (Figure 4c). Besides spheroid size, the cell viability was assessed in situ using the standard fluorescent stains for viable (calcein AM) and dead (PI) cells after 96 h of culturing (control spheroids) or 48 h culturing and 48 h paclitaxel exposure (Figure S4, Supporting Information). By releasing the spheroids, deformation of the nuclei and growth arrest could also be confirmed by off-chip light sheet microscopy. A clear change in the spheroid size, shape, and nuclei morphology was observed compared with control spheroids not exposed to paclitaxel (Figure 4d).

3. Conclusion

In this study, we took advantage of the beneficial properties of the commercial organic-inorganic hybrid polymer, Ormocomp, to set up and validate first in its kind microfluidic platform for simultaneous culturing of 2D cell monolayers and 3D cell spheroids. On one hand, the possibility to create rounded microstructures in a single lithographic step, together with subsequent lithography-based cell-repellant surface functionalization, provides substantial progress toward facile microfabrication of U-shaped microwells for 3D cell spheroid culturing under microfluidic flow. Utmost critical from the perspective of drug screening is the possibility to culture small, uniform spheroids in a reproducible manner and to release the spheroids for further off-chip analysis after drug exposure. Compared with in situ fluorescent staining, this diversifies the selection of end-points by facilitating closer examination of the spheroids by state-of-the-art off-chip cell characterization techniques and algorithm-based image analysis. On the other hand, the inherent surface properties of native Ormocomp support strong adhesion of cells and metals, which facilitates implementation of 2D cell monolayer cultures, and their non-invasive monitoring with the help of impedance spectroscopy (via integrated electrodes), on unmodified, planar parts of the same microchannel. Altogether, these technical achievements enable comprehensive evaluation of both immediate and time-dependent drug impacts on cellular events in both 2D and 3D, as shown with the help of paclitaxel in this study.

Although this work mainly focuses on performance characterization and proof-of-concept validation of the assay design (using relatively simple biological model and only a single microchannel at a time), the same microfabrication protocol is readily feasible for wafer-scale manufacturing of multiple, parallelly actuated microchannels of the same type. This is particularly important with a view to increasing the somewhat low throughput of the current assay design (only one exposure test per device) toward higher throughput screening of new drug candidates. Moreover, the microfabrication concept presented herein, provides a straightforward approach to upscaling of the number of microwells for high quantity spheroid culturing under identical flow conditions. In the present design, the microwell density was ca. 19 wells per mm^2 (for d = 200 µm well size and 30 µm well-to-well spacing), which easily outnumbers the regular wellplate set-ups in terms of spheroid production for characterization purposes. For many state-of-the-art cell characterization techniques, the number of cells needs to be much higher than that of a single spheroid. Thus, the approach presented herein, that is, culturing of multiple small spheroids under identical conditions followed by off-chip cell characterization by multiple different techniques, is capable of combining the best of both worlds (microfluidics and conventional 3D cell culturing). Despite the relatively low throughput and limited biological complexity of the current assay design, the wealth of cell-level information that can be derived from different end-point measurements (in 2D and 3D) is likely to provide a more comprehensive and accurate in vitro prediction of the in vivo drug impacts compared with current state-of-the-art cell culture methodologies.

4. Experimental Section

Microfabrication Methods and Materials: The microfluidic platforms (Figure S1, Supporting Information) were fabricated out of Ormocomp, a commercially available formulation of organically modified ceramics (Microresist Tehcnology, GmbH, Berlin, Germany), metallized using thin-film techniques, and sealed with an oxygen-permeable polydimethylsiloxane channel (PDMS, Sylgard 184, Dow Chemicals, Midland, MI). The full microfabrication process is illustrated in Figure S1, Supporting Information and elaborated below.

Defining the Microwells Out of Ormocomp for 3D Cell Spheroid Culturing: Ormocomp was spincoated and UV-cured (MA-6 mask aligner, SÜS MicroTec Inc., Garching, Germany) on 350 µm-thick Pyrex glass wafers (Plan Optik, AG, Elsoff, Germany) dehydrated in the oven (120 °C, 1 h). The first layer of Ormocomp (spin coated 6000 rpm, 30 s) was flood exposed (constant UV dose of 76 mJ cm^{-2}) and baked in the oven post-exposure (90 °C, 30 min) to yield a 15 µm-thick base layer (Figure S1A, Supporting Information). Next, the second layer of Ormocomp (800 rpm, 15 s) was UV exposed through a photomask in proximity mode (gap distance 450 µm) and baked (90 °C, 30 min) to define the microwells (Figure S1B, Supporting Information). The microwell diameter was controlled by the photomask (nominal well dimensions 125, 150, 175, and 200 µm) and the depth was controlled by the UV exposure dose (ranging between 13 and 48 mJ cm^{-2}), as illustrated in Figure 2. Finally, the Ormocomp structures were developed in OrmoDev (Microresist Technology GmbH) for 5 min, rinsed with isopropanol, dried, and hardbaked on a hotplate (200 °C, 2 h) (Figure S1C, Supporting Information). The final microdevice comprised three arrays (ca. 3.58 × 2 mm^2 cell-repellent area) of 4 × 10 microwells with 30 µm inter-well spacing.

Defining the Thin-Film Electrodes for Monitoring Cell Monolayer (2D) Integrity: For noninvasive monitoring of cell monolayer growth based on electrical impedance sensing, two pairs of thin-film gold electrodes were implemented onto the planar Ormocomp surfaces between the microwell arrays (Figure 1a). First, a 10 nm-thick titanium layer was deposited over the entire wafer by evaporation (IM-9912 evaporator, Instrumentti Mattila, Mynämäki, Finland) under same condition which pointed in Bonabi et al.[30] to promote gold adhesion onto the Ormocomp substrate (Figure S1D, Supporting Information). Next, a 100 nm-thick gold layer was deposited by evaporation (Figure S1E, Supporting Information) and patterned by photolithography. The metal pellets for evaporation (Ti and Au) were purchased from Kurt J. Lesker Company Ltd. (East Sussex, UK) and all were of 99.99–99.999% purity. A hexamethyldisilazane was applied by chemical vapor deposition (30 min) at 150 °C in the oven (Yield Engineering System, Livermore, California, USA) on top of the metallized surface to promote adhesion of the photoresist. Next, a 10 µm-thick layer of a positive tone photoresist, AZ4562 (MicroChemicals GmbH, Ulm, Germany), was spincoated (2000 rpm, 30 s) onto the metallized surface (Figure S1F, Supporting Information), softbaked on a hotplate (100 °C, 50 s), and patterned by masked UV exposure (570 mJ cm^{-2}) using the MA-6 mask aligner (Figure S1G, Supporting Information) and developed in AZ826F MIF developer (MicroChemicals GmbH, Ulm, Germany) for 3 min (Figure S1H, Supporting Information). To ensure complete removal of the photoresist also in the deep microwells, the masked UV exposure (380 mJ cm^{-2}) and development (3 min) was repeated for the second time. Afterwards, the resist was hardbaked on a hotplate (115 °C, 50 s). The nominal dimensions of the photoresist (masked) pattern comprised of two identical, semi-circular (r = 1000 µm) working and reference electrodes opposing each other, located within the microchannel, and connected through 100 µm-wide wires with contact pads (30 × 30 mm^2) residing at the sides of the chip (Figure S1, Supporting Information). This pattern was then transferred to the metal layer by sequential etching of gold in aqua regia (a mixture of 69% nitric acid and 37% hydrochloric acid, 1:3, v/v) (35 °C, 10 s) (Figure S1I, Supporting Information) and Ti in a mixture of deionized water, hydrogen peroxide and ammonium hydroxide (Honeywell, North Carolina, USA) (12:1.8:1, v/v, RT, 5 min) (Figure S1J, Supporting Information). Finally, the impedance electrodes were revealed upon resist removal (lift-off) in AZ100 remover (Microresist Technology GmbH, Berlin, Germany) (RT, 10 min) (Figure S1K, Supporting Information). The electrical resistivity of the impedance electrodes was determined by measuring the sheet resistance (RS) of the metallization with a 4-point probe (CPS probe station, Keithley 2000 multimeter, Cascade Microtech) after metal deposition but before patterning. The average value (319 ± 3 mΩ) from three measurements was then used for calculation of the bulk resistivity (ρ).

Modification of the Surface Properties to Control Cell Adherence: The inherently cell-adhesive Ormocomp surface was locally modified by oxygen plasma treatment and hydropolymer coating to create cell-repellant porous and hydrophobic surface, respectively, around the microwell arrays (Figure S1, Supporting Information). First, the cell-repellant areas (3.58 × 2 mm^2) was defined by photolithography. Briefly, a 12 µm-thick layer of the AZ4562 photoresist was spincoated (1500 rpm, 30 s) over the entire wafer, softbaked (Figure S1L, Supporting Information), patterned by masked UV exposure (twice) (Figure S1M, Supporting Information), and developed and hardbaked following protocol similar to electrode patterning (Figure S1N, Supporting Information). Only in this case, the cell-repellant areas were left unpatterned and all other areas, including the metallizations, were protected by the photoresist. To create the pores on the cell-repellant areas, the wafer was treated with oxygen plasma by reactive ion etching (200 W, 250 mTorr, O_2 flow 45 sccm, argon flow 5 sccm) for 20 min using Plasmalab 80+ (Oxford Instruments, Bristol, UK). Prior to plasma treatment, the chamber was cleaned with SF6 + O_2 plasma for 30 min. Then, a hydrophobic fluoropolymer coating was deposited by plasma-enhanced chemical vapor deposition (50 W, 250 mTorr, CHF3 flow 100 sccm, 5 min, Plasmalab 80+) (Figure S1O, Supporting Information) followed by resist removal (lift-off) in AZ 100 remover (RT, 20 min) and sequential rinsing with isopropanol and water (Figure S1P, Supporting Information).

Sealing with Polydimethylsiloxane Lid: After metallization and surface treatment, the microwell arrays and the planar, native areas with impedance electrodes were sealed with a polydimethylsiloxane (PDMS) channel (3 × 0.2 × 30 mm^3, w × h × L). The master was fabricated by spincoating SU-8 100 photoresist (Microchem Corporation, Newton, MA) on a silicon wafer (1700 rpm, 30 s) to obtain a 200 µm-thick layer. The softbake of SU-8 was done by using a slow ramp function first from RT to +65 °C and kept at +65 °C for 25 min, and then from +65 °C to +95 °C and kept at +95 °C for 3.5 h before gradual cooling to RT. Following softbake, the microchannels were patterned by UV exposure (65 s) on a mask aligner (SÜSMicroTec Inc.) after which the wafer was hardbaked by using a slow ramp function first from RT +65 °C and kept at +65 °C for 80 min and then gradually cooling to RT. Next it developed in mr-Dev 600 (Microresist technology Inc.) for 1 h. Last, the wafer was rinsed with isopropanol and dried. Finally, a fluoropolymer coating (CHF3, 100 sccm, 50 W, 250 mTorr, 10 min) was applied using PECVD (Plasmalab 80 Plus, Oxford Instruments Inc.) to act as an anti-adhesion layer.

Next, PDMS prepolymer and curing agent were mixed in a ratio of 15:1 (m/m), poured on top of the SU-8 master to reach ca. 5 mm-thick layer and degassed by placing the master in the desiccator for 1 h. To ensure good bonding strength between PDMS channel and the Ormocomp surface, PDMS was only partially cured (75 °C, 40 min) and plasma oxidized (60 W, O_2 flux 500 mL min^{-1}, 60 s, PS 400, PVA TePla, Wettenberg, Germany) prior to bonding (Figure S1Q, Supporting Information). The inlet and outlet holes were also pierced to PDMS and the Ormocomp bottom parts diced to appropriate size (DAD 3220, Disco, Tokyo, Japan) before bonding. Finally, the crosslinking of the bonded PDMS channel was completed by applying 500 gram to 1 kg weight bar on PDMS with overnight cure in the oven at 80 °C (Figure S1R, Supporting Information).

Characterization of Ormocomp Microstructures: Analysis of Microwell Size and Shape: Microwell height (n = 3 wells of each type) was determined with profilometer (Dektak XT, Bruker Inc, Karlsruhe, Germany) with 15 mg stylus force and scan resolution of 0.02 µm.

The effect of exposure dose on the microwells cross-section shape was determined from four parallel samples of each type by using scanning electron microscopy (SEM EBL Zeiss Supra 40). Before SEM analysis, all samples were sputtered by 20 nm Au (Bal-Tec SCD 050, Schalksmühle, Germany) and diced with the dicing saw to obtain cross sections. The SEM images were analyzed with Matlab to determine the radius of curvature (r), residual thickness, and height of the microwells cross-sections. The height and residual thickness determinations were a complementary method to confirm profilometer data.

Characterization of Ormocomp Microstructures: Analysis of Surface Treatment: The stability of the surface treatment over time was examined

by contact angle goniometry using the sessile droplet needle method (Theta, Biolin Scientific, Espoo, Finland). The advancing contact angles were measured from 1 to 7 µL, and the receding from 7 to 0 µL. The droplet rate was 0.1 µL s^{-1}. A clear difference between both advancing and receding contact angles were observed between native and treated surfaces and the observed change was also stable over time (Figure 2e).

Cell Maintenance: Huh7 human hepatoma cells (a kind gift from Dr. Moshe Finel, University of Helsinki, Finland) used in this study were maintained in complete growth medium consisting of high-glucose DMEM medium (Sigma, Saint Louis, MO) supplemented with 10% fetal bovine serum (Gibco, Paisley, UK), 1% non-essential amino acids (Gibco, Paisley, UK), 10 000 U mL^{-1} penicillin, and 10 000 µg mL^{-1} streptomycin (Gibco, Grand Island, NY, USA) in standard culture conditions (+37 °C, 5% CO_2, 95% humidity), and sub-cultured when reaching < 90% of confluence.

Cell Seeding to the Microchannel: Before cell seeding, the bonded microdevice was flushed first with 70% (*v*/*v*) ethanol (aq) (with at least 10× the channel volume) and then with complete growth medium. The ethanol rinse also improved the wetting of the channels thus avoiding air bubbles from trapping into the hydrophobic microwells. Next, the cells (2.5 M mL^{-1}) were loaded into the channel and allowed to adhere on native, planar Ormocomp or to sediment in microwells for 30 min, after which the flow was initiated. The flow rate used was 3.5 µL min^{-1} (5.8 mm min^{-1}) for the first 8 h, thereafter 1.4 µL min^{-1} (2.3 mm min^{-1}). The growth medium consisted of the complete medium supplemented with 2% (*v*/*v*) Geltrex (Geltrex LDEV-Free Reduced Growth Factor Basement Membrane Matrix, Gibco, Grand Island, NY), to promote spheroid formation in the microwells as it provides with the ECM components to 3D cultures.

On-Chip Imaging: During incubation spheroid growth was monitored online using Cytosmart camera and Cytosmart Lux2 software (Incyte, the Netherlands). At chosen end points (24, 48, 72, and 96 h), the microdevices were removed from the incubator, and the cells were imaged, and stained using Calcein AM (1 µM, Invitrogen, Eugene, OR), PI (2 drops per mL, ReadyProbes Reagent, Invitrogen, Eugene, OR), and Hoechst 33 342 (2 drops per mL, NucBlue Live ReadyProbes Reagent, Invitrogen, Eugene, OR) for live cells, dead cells, and all nuclei, respectively. The cells were imaged using either AxioVert A1 FL epifluorescence microscope (Zeiss Finland, Espoo, Finland) equipped with a broadband lamp (Illuminator HXP 120 V, Leistungselektronik JENA GmbH, Jena, Germany) and Axiocam 305 microscope camera (Zeiss Finland, Espoo, Finland), or AxioScope A1 epifluorescence upright microscope (Zeiss Finland, Espoo, Finland) equipped with halogen broadband lamp (HAL 100, Zeiss) and Retiga 4000R CCD camera (Q Imaging, Surrey, BC, Canada). All images were analyzed with ImageJ freeware.

On-Chip Impedance Spectroscopy: The cell monolayer growth was monitored with help of impedance spectra recorded once every hour (44 data points between 5–100 000 Hz, U_{AC} = 10 mV) using PalmSens4 potentiostat (PalmSens BV, Houten, the Netherlands). Impedance of cell covered electrode versus cell-free electrode were extracted from the data, and maximum signal was detected at frequency of 16 kHz, thus this was considered the optimal frequency[33] to monitor the hepatocyte monolayer integrity upon cell culturing and drug exposure in this particular system.

Flow Cytometric Analysis: Cell cycle analysis was assessed with help of flow cytometry. For the flow cytometric analyses spheroids chips with 4 × 85 well arrays with a single well diameter (all d = 200 µm with 30 µm inter-well spacing, comprised of no planar areas) were used to ensure >10 000 events for the analysis. The cell count resulting from the on-chip cell monolayer cultures was not high enough for flow cytometry analysis, and thus, the drug effects on cell monolayer cultures were assessed on the basis of conventional microtiter plate cultures. For flow cytometric analysis, the spheroids were flushed out of the microchannel and dissociated with Accutase (Invitrogen, Carlsbad, CA). Dissociation of spheroids into a homogenous cell suspension was achieved upon 20–30 min incubation at +37 °C aided by brief mixing with a pipette every 10 min. After dissociation, the cells were washed and fixed with ice-cold 70% (*v*/*v*) ethanol (aq) over night. For cell cycle analysis, the cells were stained with FxCycle RNase/PI staining solution (Invitrogen, Eugene, OR) according to the manufacturer's instruction, and analyzed with BD Accuri Flow Cytometer (BD bioscience, Franklin Lakes, New Jersey). Monolayer cells were dissociated for 10 min using Accutace, and onwards, handled similarly to dissociated spheroid cells. FloJo software (FloJo LLC, Ashland, Oregon) was used for data analysis.

Light Sheet Microscopy: Detailed analysis of spheroid structures was done off-chip using a Zeiss LightSheet Z.1 microscope (Zeiss) with filter set of BP505-545 LP660 404900–9318 and 20×/1.0 dipping water objective. Spheroids smaller than 100 µm in diameter were flushed off-chip, fixed in 4% paraformaldehyde (PFA) for 15 min, following with permeabilization in 0.5% Triton-X 100 for 15 min (RT), and blocking in 3% bovine serum albumin (fraction V, de-lipidated, New Zealand source in DPBS) (Image-iT Fixation/Permeabilization Kit, Invitrogen, Grand Island, NY). Spheroids larger than 100 µm in diameter were flushed off-chip, fixed and permeabilized simultaneously in a mixture of 2% PFA and 0.25% (*v*/*v*) Triton-X 100 for 3 h (RT). Actin was stained using ActinGreen 488 ReadyProbes Reagent (Invitrogen, Eugene, OR) and nuclei with 10 µM DRAQ-5 (Thermo Scientific, England, Scotland, UK) over night (+4 °C). The spheroids were mounted in TopVision low-melting point agarose (Thermo Scientific) and imaged in phosphate-buffered saline. Every spheroid was imaged using 0.47 µm stack heights and dual side illumination. Image analysis was done with IMARIS 9.2.1. software.

Statistics: Data are expressed as mean ± SD, as is also indicated in the figure legends. Linear regression or Pearson's correlation (two-tailed, data normality tested with Shapiro–Wilk) were used in the validation studies (Figures 3b,c, respectively). Drug impact on spheroid size was compared pair-wise as independent samples using the Kruskal–Wallis test (asymptotic significances, 2-tailed tests, significance values were adjusted by the Bonferroni correction for multiple tests) (Figure 4c). Data in Figure 4c are presented as box-and-whisker plots in which the boxes indicate the first and third quartiles with median, the upper and lower bars minimum and maximum values, and the circles outliers. Statistical analysis was done with IBM SPSS statistics 25.

Supporting Information

Supporting Information is available from the Wiley Online Library or from the author.

Acknowledgements

P.J. and A.B. contributed equally to this work. The work was financially supported by the European Research Council (grant no. 311705/CUMTAS), the Academy of Finland (grants no. 308911 and 309608), and the Magnus Ehrnrooth foundation (P.J.). The Micronova, Center for Micro and Nanotechnology and the Light Microscopy Unit, Institute of Biotechnology, are acknowledged for access to cleanroom microfabrication and light sheet microscopy facilities, respectively.

Conflict of Interest

The authors declare no conflict of interest.

Keywords

3D cell culturing, microfluidics, microwells, organically modified ceramics, organ-on-a-chip devices

Received: January 17, 2020
Revised: February 20, 2020
Published online: March 12, 2020

[1] K. Duval, H. Grover, L. H. Han, Y. Mou, A. F. Pegoraro, J. Fredberg, Z. Chen, *Physiology* **2017**, *32*, 266.
[2] J. M. Lee, P. Mhawech-Fauceglia, N. Lee, L. C. Parsanian, Y. G. Lin, S. A. Gayther, K. Lawrenson, *Lab. Invest.* **2013**, *93*, 528.
[3] F. Pampaloni, E. G. Reynaud, E. H. Stelzer, *Nat. Rev. Mol. Cell Biol.* **2007**, *8*, 839.
[4] V. M. Weaver, S. Lelievre, J. N. Lakins, M. A. Chrenek, J. C. Jones, F. Giancotti, Z. Werb, M. J. Bissell, *Cancer Cell* **2002**, *2*, 205.
[5] E. T. Verjans, J. Doijen, W. Luyten, B. Landuyt, L. Schoofs, *J. Cell. Physiol.* **2018**, *233*, 2993.
[6] C. J. Lovitt, T. B. Shelper, V. M. Avery, *BMC Cancer* **2018**, *18*, 41.
[7] P. Godoy, N. J. Hewitt, U. Albrecht, M. E. Andersen, N. Ansari, S. Bhattacharya, J. G. Bode, J. Bolleyn, C. Borner, J. Bottger, A. Braeuning, R. A. Budinsky, B. Burkhardt, N. R. Cameron, G. Camussi, C. S. Cho, Y. J. Choi, J. Craig Rowlands, U. Dahmen, G. Damm, O. Dirsch, M. T. Donato, J. Dong, S. Dooley, D. Drasdo, R. Eakins, K. S. Ferreira, V. Fonsato, J. Fraczek, R. Gebhardt, et al., *Arch. Toxicol.* **2013**, *87*, 1315.
[8] M. Vinci, S. Gowan, F. Boxall, L. Patterson, M. Zimmermann, W. Court, C. Lomas, M. Mendiola, D. Hardisson, S. A. Eccles, *BMC Biol.* **2012**, *10*, 29.
[9] S. Nath, G. R. Devi, *Pharmacol. Ther.* **2016**, *163*, 94.
[10] M. E. Boutin, T. C. Voss, S. A. Titus, K. Cruz-Gutierrez, S. Michael, M. Ferrer, *Sci. Rep.* **2018**, *8*, 11135.
[11] L. D. Ma, Y. T. Wang, J. R. Wang, J. L. Wu, X. S. Meng, P. Hu, X. Mu, Q. L. Liang, G. A. Luo, *Lab Chip* **2018**, *18*, 2547.
[12] B. Patra, C. C. Peng, W. H. Liao, C. H. Lee, Y. C. Tung, *Sci. Rep.* **2016**, *6*, 21061.
[13] M. Rothbauer, H. Zirath, P. Ertl, *Lab Chip* **2018**, *18*, 249.
[14] S. Sart, R. F. Tomasi, G. Amselem, C. N. Baroud, *Nat. Commun.* **2017**, *8*, 469.
[15] L. B. Weiswald, J. M. Guinebretiere, S. Richon, D. Bellet, B. Saubamea, V. Dangles-Marie, *BMC Cancer* **2010**, *10*, 106.
[16] I. Smyrek, E. H. Stelzer, *Biomed. Opt. Express* **2017**, *8*, 484.
[17] K. Moshksayan, N. Kashaninejad, M. E. Warkiani, J. G. Lock, H. Moghadas, B. Firoozabadi, M. Saidi Said, N. Nguyen, *Sens. Actuators, B* **2018**, *263*, 151.
[18] J. P. Camp, T. Stokol, M. L. Shuler, *Biomed. Microdevices* **2008**, *10*, 179.
[19] T. Y. Tu, Z. Wang, J. Bai, W. Sun, W. K. Peng, R. Y. Huang, J. P. Thiery, R. D. Kamm, *Adv. Healthcare Mater.* **2014**, *3*, 609.
[20] G. J. Wang, K. H. Ho, S. H. Hsu, K. P. Wang, *Biomed. Microdevices* **2007**, *9*, 657.
[21] T. Sikanen, S. Aura, L. Heikkilä, T. Kotiaho, S. Franssila, R. Kostiainen, *Anal. Chem.* **2010**, *82*, 3874.
[22] F. Klein, B. Richter, T. Striebel, C. M. Franz, G. von Freymann, M. Wegener, M. Bastmeyer, *Adv. Mater.* **2011**, *23*, 1341.
[23] E. Käpylä, A. Sorkio, S. Teymouri, K. Lahtonen, L. Vuori, M. Valden, H. Skottman, M. Kellomäki, K. Juuti-Uusitalo, *Langmuir* **2014**, *30*, 14555.
[24] S. Schlie, A. Ngezahayo, A. Ovsianikov, T. Fabian, H. A. Kolb, H. Haferkamp, B. N. Chichkov, *J. Biomater. Appl.* **2007**, *22*, 275.
[25] S. Turunen, T. Joki, M. L. Hiltunen, T. O. Ihalainen, S. Narkilahti, M. Kellomäki, *ACS Appl. Mater. Interfaces* **2017**, *9*, 25717.
[26] S. H. Yoon, Y. K. Kim, E. D. Han, Y. H. Seo, B. H. Kim, M. R. Mofrad, *Lab Chip* **2012**, *12*, 2391.
[27] A. Bonabi, S. Cito, P. Tammela, V. Jokinen, T. Sikanen, *Biomicrofluidics* **2017**, *11*, 034118.
[28] S. O. Oliveira, W. Song, N. M. Alves, J. F. Mano, *Soft Matter* **2011**, *7*, 8932.
[29] V. Jokinen, E. Kankuri, S. Hoshian, S. Franssila, R. H. A. Ras, *Adv. Mater.* **2018**, *30*, 1705104.
[30] A. Bonabi, S. Tähkä, E. Ollikainen, V. Jokinen, T. Sikanen, *Micromachines* **2019**, *10*, 605.
[31] S. Aura, V. Jokinen, M. Laitinen, T. Sajavaara, S. Franssila, *J. Micromech. Microeng.* **2011**, *21*, 125003.
[32] M. A. Jordan, R. J. Toso, D. Thrower, L. Wilson, *Proc. Natl. Acad. Sci. U. S. A.* **1993**, *90*, 9552.
[33] J. A. Stolwijk, K. Matrougui, C. W. Renken, M. Trebak, *Pflügers Arch.* **2015**, *467*, 2193.